Foldable Electrochromics Enabled by Nanopaper Transfer Method

*Wenbin Kang, Chaoyi Yan, Ce Yao Foo, and Pooi See Lee**

An innovative nanopaper-transfer method enabled by the high surface free energy of nanocellulose is reported. Utilizing this technique, Ag nanowire percolating network based transparent conductive electrodes with ultrahigh figure of merit are realized. With the exceptional surface properties of this novel nanopaper electrode, a foldable electrochromic nanopaper device with a stable performance is demonstrated for the first time. This nanopaper-transfer technique holds great promise for the next generation deformable electronics.

1. Introduction

Electrochromism is defined as reversible change of colors under supplied voltage.[1] The requirement for electrochromic materials is the existence of electrochemical redox reactions coupled with modulation of light transmittance upon voltage application. There are various ways to fabricate electrochromic electrodes among which the solution processible manner is very promising and most often adopted with attractive properties such as fast switching, ease of coating on nonconformable substrates, facile and low cost fabrication.[2] Electrochromism has been frequently utilized for different applications such as smart window in buildings, paper-like reflective display, antiglare mirrors, etc. However, the functionality of general electrochromic devices has been limited to a simple light modulation at stand-still state like on glass or at most a flexible state on polyethylene terphthalate (PET). More diversified functionalities such as stretchability or foldability have to be developed to meet the stringent requirements of future emerging applications.[3]

Electrochromic devices and many other electronics, optoelectronics, or touch devices require the use of transparent conducting electrodes (TCEs). The commonly used commercial conductive material is indium tin oxide (ITO). The problems of scarcity of indium, fluctuating cost, brittleness under deformation, have prompted an urgent need to find alternative materials for emerging and futuristic devices. The pursuits of an electrode with high transparency and conductivity have been a challenging task. Efforts have been channeled into adopting carbon nanotube (CNT),[4,5] graphene,[6–8] metallic wires network,[9–12] metal grids,[13,14] and hybrid electrodes[15,16] to make transparent conductive electrodes. Ag nanowires with large aspect ratios have been reported to be one of the most promising candidates to compete with ITO.[9,17,18] The high aspect ratio of nanowires promotes easy interconnection and good endurance to physical deformations such as bending, stretching, and folding.[16,19,20] However, the transparency and conductivity of Ag nanowire based electrodes still require further optimization in order to achieve a higher figure of merit (FOM) to cater for more stringent requirements for devices of the next generation. Besides, alternative substrates have to be developed in order to bestow the future TCE with more complex functionalities like stretchability and foldability.

Conventional flexible transparent conductive electrodes have been dominated by plastics such as polyethylene terephthalate (PET), polyimide (PI), or polycarbonate (PC). A rising concept of adopting nanocellulose based electrode has stirred excitement in anticipation of sustainable electronics. Its ubiquitous source, recyclable, biocompatible, and degradable nature has rendered the concept of nanopaper electrode well received. Cellulose can be disintegrated into nanoscale through physical liberation,[21] tempo-oxidation,[22] enzyme treatment,[23] $NaClO_4$ induced surface charge separation,[24] and so forth. When the size shrinks to nanoscale, enhanced fiber interaction leads to high mechanical strength;[25] and the smaller diameter is beneficial for reduced back light scattering[26] and thus an enhanced transparency. The excellent thermal stability (>180 °C) and low coefficient of thermal expansion of 5–10 ppm K^{-1} ensures an excellent processibility and compatibility with a broad range of processing techniques.[27] The hydrophilic surface of nanopaper is also beneficial for printing, which makes it an excellent choice for printed electronics and it is very promising for industrial scale up.[28] The hydrophilic nanopaper could act as electrolyte reservoir, advantageous for enhanced electrochemical reactions.[29,30] In this work, we developed a novel nanopaper transfer method (procedure shown in **Figure 1**a) and realized the concept of foldable electrochromics based on this transfer method. The approach is enabled by the high surface free energy of nanocellulose coupling the strong van der Waals force that stems from the surface of the nanopaper substrates.

W. Kang, Dr. C. Yan, C. Y. Foo, Prof. P. S. Lee
School of Materials Science and Engineering
50 Nanyang Avenue, 639798, Singapore
E-mail: pslee@ntu.edu.sg

DOI: 10.1002/adfm.201500527

2. Results and Discussion

The transparent nanopaper is made of nanocellulose which is physically liberated from regular sized cellulose fiber bundles into nanofibrils. The diameters of the nanocellulose nanofibrils

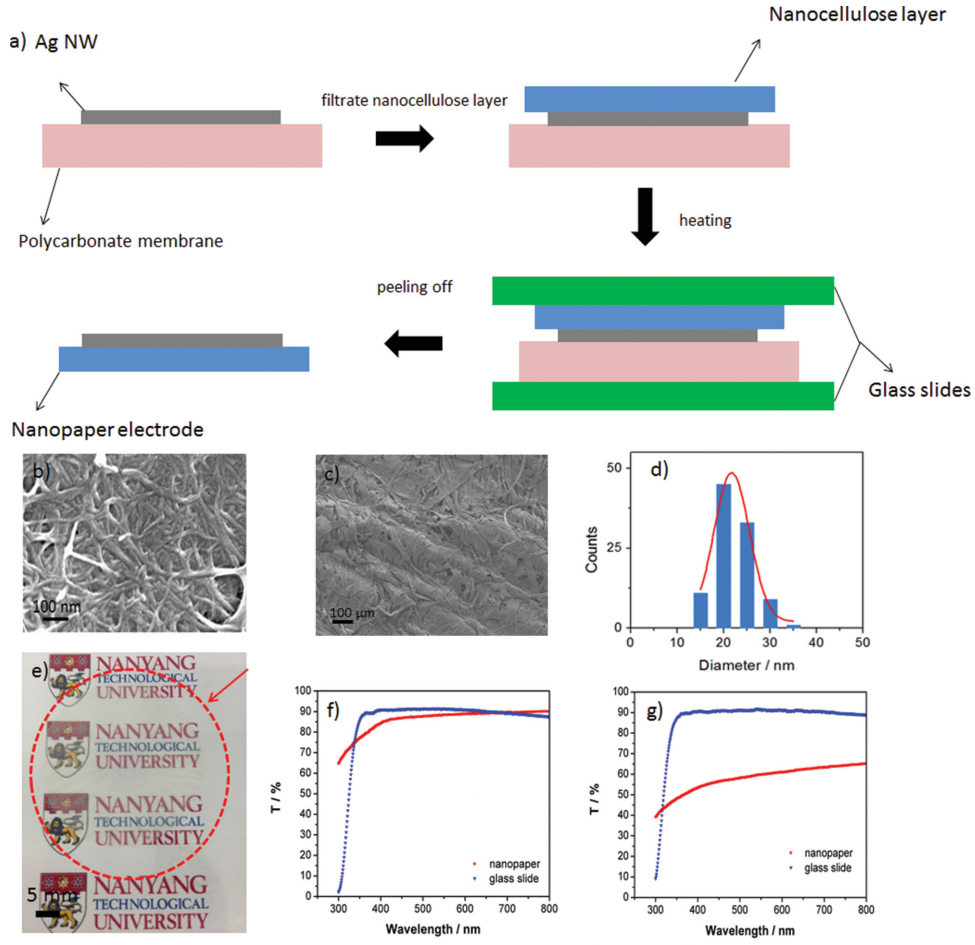

Figure 1. Procedures to fabricate the transparent conductive nanopaper electrode utilizing the nanopaper transfer method shown in (a); and b) nanopaper surface with a dense layers of assembled nanocellulose fibrils; c) a regular Kim wipe paper with large fiber diameters of 15–60 μm; d) the diameter distribution of the nanopaper fibrils; e) digital image of the highly transparent nanopaper; f) the transparency of nanopaper compared to glass slide at 0 mm distance away and g) 20 mm away from the detector.

are around 22 nm and the nanopaper is much denser than a regular paper (Figure 1b–d). The strong fiber interaction makes the nanopaper extremely tough with Young's modulus reaching 20 GPa (Figure S1, Supporting Information). In terms of the optical property, a small size in diameter below visible light wavelength is beneficial for reduced light scattering from a single fiber.[26,31,32] There are also much fewer pores inside the nanopaper structure with less air trapped in the cavities and thus much fewer scattering points.[33,34] Typically a regular paper delivers an opaque nature, but the nanofibril renders the nanopaper highly transparent (Figure 1e). The diffusive transmittance of our nanopaper was measured to be 88.1% at 600 nm wavelength at 0 mm distance from the light source detector. The transmittance is close to that of a glass slide of 90.9% (Figure 1f), but with an advantage of the elimination of the low end (300 nm) absorption edge inherent in the glass slide and PET[35] substrates. When the distance increases to 20 mm away from the detector, the transmittance value dropped to 60.8% due to the haze effect (Figure 1g and Figures S2–S4, Supporting Information). While low haze substrate with little scattering may be required for high clarity display systems, a high haze value is beneficial for thin film solar cells, antiglare display, reflective reading, etc.[26,33,34] A low haze factor can be achieved with the use of tempo-treated nanopaper or $NaClO_4$-treated nanopaper that gives less than 6% haze.[24,36]

To make the transparent nanopaper conductive, we adopted a novel nanopaper transfer method. Different from traditional dry transfer[37–43] (transfer materials covered in the literature include single wall carbon nanotube (SWCNT), graphene, Ag nanowire), a donor substrate or "stamp" with low surface energy is a prerequisite (typically it is polydimethylsiloxane (PDMS)) for a successful transfer to the destination substrate. The nanopaper transfer method is able to work with various stamps with wider range of surface energy levels and it is very efficient so as to achieve a clean transfer. To explain this, Dupre equation[44,45]

$$W_{AB} = \gamma_A + \gamma_B - \gamma_{AB} \quad (1)$$

(where W_{AB} is the work of adhesion; γ_A, γ_B, γ_{AB} refer to surface free energy of A, surface free energy of B, and the interfacial free energy between A and B) as well as a model to estimate the interfacial free energy needs to be considered. By solely considering London dispersion force which is most generally adopted for intermolecular forces[38,46]

$$\gamma_{AB} = \gamma_A + \gamma_B - 2\sqrt{\gamma_A \gamma_B} \quad (2)$$

thus

$$W_{AB} = 2\sqrt{\gamma_A \gamma_B} \quad (3)$$

For a successful transfer, the work of adhesion between the destination substrate and the transfer material must be larger than that between the material and the stamp. It is thus required that the destination substrate has a larger surface free energy than the stamp.

The nature of the high surface energy of nanocellulose is most critical to facilitate this transfer process. The existence of abundant free hydroxyl groups on cellulose surface contributes to a high surface energy.[47,48] The liberation of regular cellulose bundles into cellulose nanofibrils greatly increases the amount of free hydroxyl groups when fine fibers are cleaved from big bundles exposing new surfaces. In addition, part of the amorphous regions was removed during nanocellulose liberation process, which would also contribute to an enhanced surface energy.[49] The comparison of nanocellulose surface free energy with some frequently used materials is listed in Table S1, Supporting Information. The surface of nanocellulose is polar, the previously mentioned model has underestimated the presence of Keesom or Debye intermolecular forces from dipole–dipole interactions.[38,50] Thus the work of adhesion from nanocellulose surface makes it very favorable for the transfer.

It is noteworthy that our successful transfer demonstrations are carried out using polycarbonate surface (the stamp) which has a high surface free energy of 42.3 mJ m^{-2}. As illustrated in Figure S5 (Supporting Information), when PDMS (low γ_s) is used as the destination substrate, it failed to pick-up transfer materials from polycarbonate (high γ_s). In another control experiment, nanopaper (high γ_s) can easily pick-up transfer materials from polytetrafluoroethylene (PTFE) (low γ_s) even under a simple pen drawing pressure. Due to the exceptional surface energy of nanocellulose, the nanopaper-transfer method is versatile in transferring various nanostructured materials like Ag nanowire, single wall CNT, and ZnO nanoparticles (Figure S6, Supporting Information).

We conducted a series of transfer for Ag nanowires of various amount to obtain transparent conductive nanopaper electrodes with different transmittance and conductivity. Ag nanowire diluted to 0.025 mg mL^{-1} in ethanol is adopted for the filtration. The amount used ranged from 0.5 to 10 mL and the resulted electrode delivered sheet resistance ranging from 630 to 0.75 Ω sq^{-1}. The transmittance spectra shown in **Figure 2**a shows that samples with lower sheet resistance give lower transmittance. This is expected since lower sheet resistance is resulted from a denser network (Figure 2d–f) that permits less light transmission. A comparison on the optical property between ITO/glass (15 Ω sq^{-1}) and our nanopaper electrode is shown in Figure 2c. For nanopaper electrode, a small hump at around 330 nm is due to the characteristic plasma frequency of Ag.[15] Due to the large aspect ratio of the Ag nanowires, only the transverse resonance peak is observed in the UV–vis region.[51,52]

The transmittance value (taken at 600 nm) with the corresponding sheet resistance is listed in **Table 1**. Figure 2b shows the relationship between transparency versus sheet resistance for nanopaper electrodes fabricated using varied amount of Ag nanowire. At the higher sheet resistance end, a small drop in transparency is able to bring about a large increase in conductivity. This is due to the loosely distributed Ag nanowires at this regime, a small increase of Ag nanowire will largely enhance

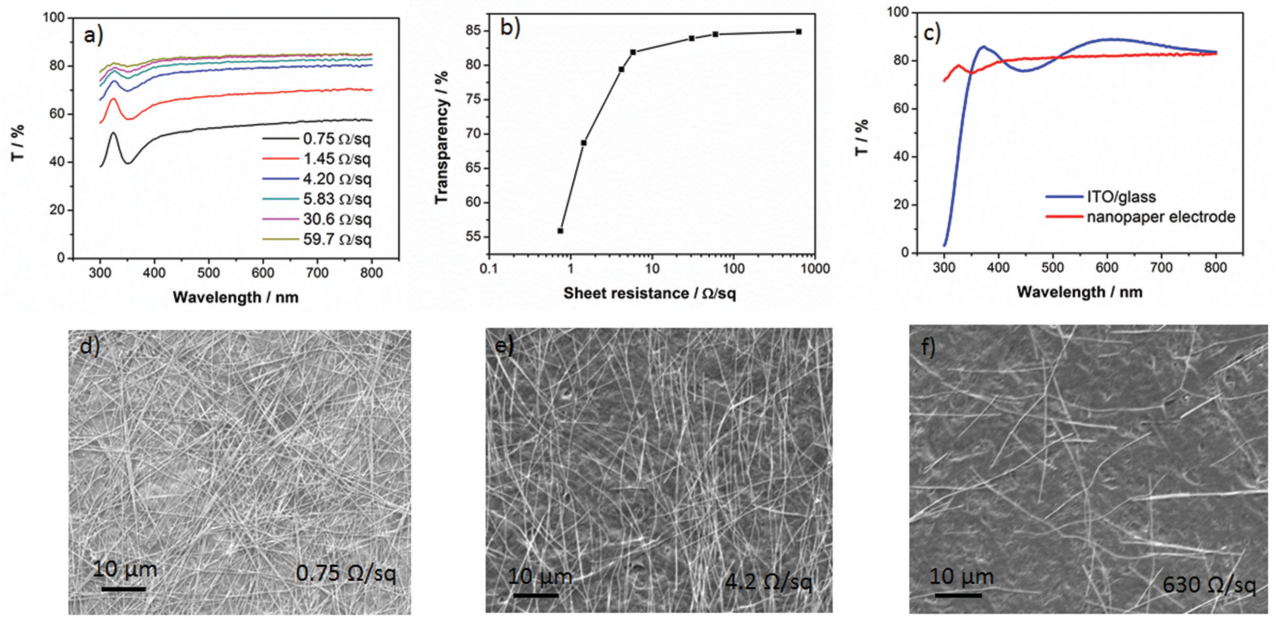

Figure 2. The relationship between optical and electrical properties of nanopapers as well as the FESEM images for corresponding Ag nanowire networks. a) Spectra of nanopaper electrodes of different sheet resistance (spectrum of the 630 Ω sq^{-1} sample is almost overlapping with the 59.7 Ω sq^{-1} sample); b) transparency (600 nm) at different sheet resistance values; c) transparency comparison between a nanopaper electrode (5.83 Ω sq^{-1}) and a commercial ITO/glass (15 Ω sq^{-1}); d–f) FESEM images of the Ag nanowire networks of different sheet resistance.

Table 1. Transparency and figure of merit values for samples of different sheet resistance.

Sample [Ω sq^{-1}]	0.75	1.45	4.2	5.83	30.6	59.7	630
Transparency %, 600 nm	55.9	68.8	79.4	81.9	83.9	84.5	84.9
Transparency subtracting nanopaper background %, 600 nm	63.5	78.1	90.1	92.9	95.2	95.9	96.4
F.o.m	986.0 bulk	988.2 bulk	838.8 percolative	862.0 percolative	247.4 percolative	149.3 percolative	16.2 percolative

the interconnection. However, at the low sheet resistance end, a large drop of transparency will result in very limited increase in conductivity, which is due to the highly interconnected state of Ag nanowires network that is insensitive to additional Ag nanowires.

To determine the quality of the electrode, figure of merit (F.O.M), that is σ_{dc}/σ_{op} (Equation (4)) has been commonly adopted.[17,53,54] σ_{dc}, σ_{op} of conductive layers follow the theoretical equation[55] (Equation (5)) in which σ_{dc}, σ_{op}, μ_0, ε_0 refer to DC conductivity, optical conductivity, permeability of free space, permittivity of free space, respectively

$$\text{F.O.M.} = \frac{\sigma_{dc}}{\sigma_{op}} \tag{4}$$

$$T = \left(1 + \frac{1}{2R_s}\sqrt{\frac{\mu_o}{s_o}}\frac{\sigma_{op}}{\sigma_{dc}}\right)^{-2} = \left(1 + \frac{188.5}{R_s}\frac{\sigma_{op}}{\sigma_{dc}}\right)^{-2} \tag{5}$$

As shown in Table 1, a high F.O.M of 988 can be achieved, this exceeds the previous best reported F.O.M. of 500.[54] The reason for the ultrahigh F.O.M is related to the nature of the nanopaper transfer process. Previous research on Ag nanowire network is mostly based on PET or glass substrates. Ag nanowires that are roll coated,[9] or spin coated,[15] get interconnected after the solvent evaporates. Herein, our paper transfer method incorporates a simultaneous assembly process of nanocellulose fibrils aggregating into a dense paper substrate accompanying the evaporation of water due to the strong hydrogen bonding interaction between fibrils. After the water evaporates, the nanopaper layer endures shrinkage of size (6% reduction in diameter) and the Ag nanowire will be forced closer and the connectivity and thus conductivity will be enhanced. This is proven by the reduction in sheet resistance (38.6% reduction based on a sample of 0.61 Ω sq^{-1}) before and after the nanopaper transfer process. F.O.M will largely be dependent on the extent each wire can interact, with better interaction or equally less junction resistance,[56] F.O.M would correspondingly be higher. Therefore the nanopaper transfer process results in an excellent conductivity and thus a high F.O.M value.

In the determination of the F.O.M of a TCE system, this value would be a constant once the conductive materials and fabrication process have been defined. The F.O.M value should be determined after the percolation-bulk transition has been completed (the validity of this theory is provided in the supporting information). If the T-R_s data is still in the percolative region, it should be best modified with the percolative theory as shown in the supporting information. We have thus indicated the bulk/percolative data points in Table 1 to make a distinction.

The soft metallic Ag nanowire network structure overcomes the brittleness problem for ITO. We demonstrate the foldability of the nanopaper electrode by repeated folding and track the change of sheet resistance accordingly (the thickness of the nanopaper is around 15 μm and the radius of curvature after folding is around 5 μm as shown in Figure S7, Supporting Information). When the nanopaper was folded with Ag nanowire pushed face to face, that was defined as −180° folding; when folded with Ag nanowire back to back, it was defined as +180° folding (**Figure 3**a). The test was carried out in a continuous manner with the nanopaper electrode cycled 100 times to −180° first before it is subjected to another 100 times cycle to +180° as is illustrated in Figure 3a. The original sheet resistance for the selected nanopaper electrode for the folding test is 0.68 Ω sq^{-1}. Even after 200 cycles of folding, the conductivity of the nanopaper electrode still maintains at a high level below 1 Ω sq^{-1}. The foldability of the nanopaper electrode is due to several reasons as seen in Figure 3b,c. First, the Ag nanowire is conformally covering the nanopaper surface and the adhesion is strong enough to accommodate displacement from structure deformation; even after the creases are formed after the folding, Ag nanowires still adhere strongly. The soft metallic nature of Ag nanowire enables it to bend accordingly with crease formed. Finally the long nanowire structure is able to maintain interconnectivity under structure deformation. The foldability of the conductive nanopaper electrode is visually reflected in a circuit connection experiment to light LED bulbs before and after crumpling as is seen in Figure 3e,f.

With these advanced properties of the novel nanopaper electrode, it is highly suited for various foldable electronic applications. To demonstrate one, we realized the concept of electrochromic nanopaper with an excellent performance. A digital image of electrochromic nanopaper at bleached and colored states is shown in **Figure 4**a,b. The pattern of the nanopaper electrode comes from the filtration of Ag nanowire through a lithographically cut PDMS mask. After deposition of WO_3, a well functioned electrochromic nanopaper with desired pattern was successfully fabricated.

WO_3 is an electrochromic material that reversibly changes its color (or reflectance) with voltage input supplied. For WO_3 in H_2SO_4 electrolyte, the electrochromic mechanism can be simply described in Equation (6)

$$WO_{3(\text{bleached})} + n\,e^- + n\,H^+ \leftrightarrow H_n WO_{3(\text{colored})} \tag{6}$$

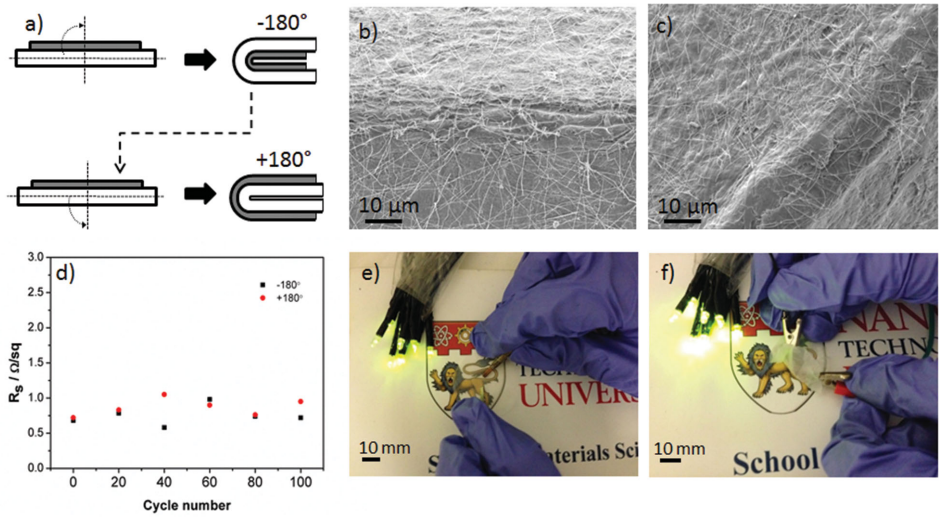

Figure 3. Foldability test of the nanopaper electrode. a) Schematics for the folding procedure; FESEM images of the nanopaper electrode folded to b) −180° and c) +180°; d) sheet resistance versus cycling with 100 cycles to −180° and another 100 cycles to +180° conducted in a consecutive manner; digital images of the foldability test of Ag nanowire nanopaper electrode connected in a circuit with LED bulbs e) before crumpling and f) after crumping.

The change of color would be reflected in the spectrum change. We referenced the WO_3 coated nanopaper electrode as the background, thus any change to the spectrum is due to the color change of WO_3.

The electrochromic nanopaper offers an obvious color change and the contrast is taken at 633 nm which is widely adopted to reflect WO_3 contrast and around which the highest contrast of the electrochromic nanopaper is observed. The contrast is 41% for this nanopaper (Figure 4c). The spectrum of the colored state features two regions: from 300–400 nm, the enhanced reflectance is due to the blue color nature of reduced WO_3 that reflects strongly at the short wavelength region; from 400 to 800 nm, the absorption of longer wavelength decreases the reflectance intensity.

The switching time is defined as the time consumed for 90% completion of the contrast modulation. From Figure 4e, a fast coloring and bleaching time is determined to be 11.8 and 20.1 s, respectively.

One of the most important properties for electrochromic materials to be considered is the cycling stability. For inorganic metal oxide materials, the color switching process is always coupled with the intercalation and de-intercalation process of ions from electrolyte into/out of the inorganic lattice structures. During these processes, the electrochromic materials would expand and undergo structure deformation which often results in the peel-off of the active films.[2,57] It has been proven that soft paper surface that can be shaped into a wrinkled structure

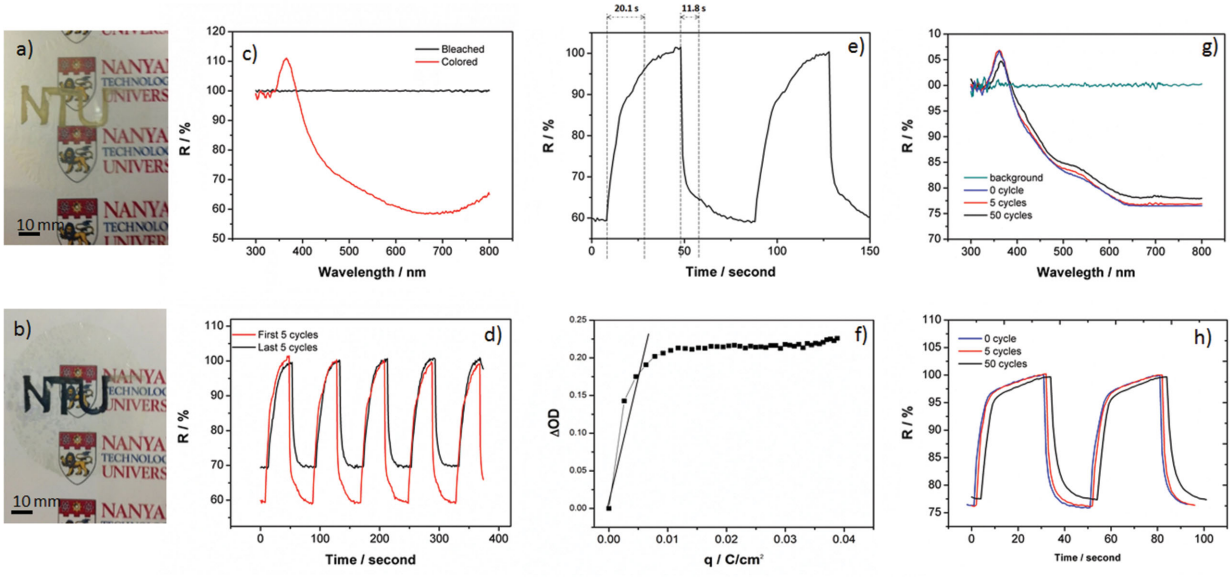

Figure 4. Electrochromic performance of the WO_3 deposited nanopaper electrode. Digital images of the electrochromic nanopaper at a) bleached state and b) colored state; c)contrast measurement; d) cycling stability test (500 cycles); e) switching rate test; f) coloration efficiency calculation; g) folding influence on contrast; h) folding influence on switching rate.

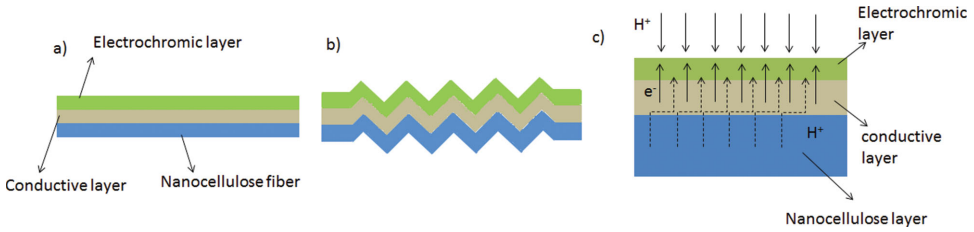

Figure 5. Schematics for the mechanism of enhanced cycling stability by forming a wrinkled structure a) before and b) after H^+ intercalation. c) Schematic for the double electrolyte injection pathway for nanopaper substrate.

is very effective in alleviating the intercalation stress and it is very useful to enhance electrochemical properties.[29,30] We obtained a very stable cycling behavior with only 22% contrast loss even after 500 cycles as seen in Figure 4d. To make a comparison, we referenced our previously published data[3] in which a Ag nanowire network is embedded in PDMS matrix for stretchable electrochromics which suffers a quick drop of contrast of around 20% after 100 cycles. The schematic representation on how the electrochromic nanopaper undergoes the stress alleviating process is shown in **Figure 5**a,b, depicting the soft fiber surface accommodating electrochemically resulted strain from H^+ intercalation by forming wrinkles, preventing the delamination of the electrochromic layer.

Apart from the enhanced electrochemical cycling stability, the nanopaper electrode is also beneficial for other electrochemical properties such as an enhanced electrochemical deposition coverage and a better coloration efficiency.

Figure S8a,b (Supporting Information) shows the coverage of electrodeposited WO_3 on nanopaper electrode. WO_3 not only covers Ag nanowire that is conductive but also fills the open space between nanowires. The highly hydrophilic hydroxyl groups of the nanocellulose serve as a reservoir for peroxotungstic acid (PTA) precursor and the hydrophilic surface will readily accommodate and anchor freshly deposited WO_3. Due to the negative polarity condition, as soon as WO_3 is deposited it will be reduced to intercalated states with additional electrons charging to the conduction band behaving as free electrons, WO_3 will experience a large increase in conductivity at this stage.[58,59] Continuous electrons supply from the negative voltage supply promotes lateral growth and the uniform coverage of WO_3 across the whole electrode surface.

Furthermore, the hydrophilic nanopaper that serves as an electrolyte reservoir can boost the coloration efficiency of the electrochromic film. Coloration efficiency is defined in Equation (7)

$$\eta = \Delta OD/q;\ \Delta OD = \log\left(R_{bleach}/R_{colored}\right) \quad (7)$$

Herein, R_{bleach} and $R_{colored}$ refer to the sample reflectance at the bleaching and colored state, respectively. ΔOD indicates the change of optical density and q refers to charge inserted to WO_3 per unit area. Coloration efficiency is to determine the extent color can change with unit charge per area supplied. A higher η value indicates better readiness for the electrochromic film to change color. A high coloration efficiency value of 34.8 $cm^2\ C^{-1}$ is achievable as seen from Figure 4f. The coloration efficiency has increased by three fold as compared to the PDMS hydrophobic electrode.[3] The much higher efficiency for the electrochromic nanopaper is due to two possible reasons. First, the hydrophilic nanofiber network with tiny pores stores electrolyte (acts as electrolyte reservoir) and provides an additional intercalation pathway as compared to PDMS based electrode. This enables the electrochromic nanopaper to change color from inside and outside at the same time (schematic shown in Figure 5c). Besides, a more uniform coating ensures a better modulation of light (detailed explanation in the Supporting Information). The above-mentioned points eventually result in the electrochromic nanopaper electrode with three fold enhancement in coloration efficiency.

We have also carried out a folding test and studied its influence on the electrochromic performance of our nanopaper device. The electrodeposition time was reduced from 100 to 30 s to lower the film thickness (from 3.4 µm in Figure S8c (Supporting Information) to about 1.6 µm in Figure S8d (Supporting Information)) to reduce internal folding stress for a better foldability.

We fixed the folding pattern with "face to face" (–180°) (Figure S8g, Supporting Information) to demonstrate the foldability. The electrochromic performance of the device was recorded at 0, 5th, and 50th folding cycles. From the optical modulation contrast study as shown in Figure 4g, the device delivers a contrast of 23.2% at the wavelength of 633 nm before folding (the contrast is lower due to the reduced thickness). The 5 folding cycles leaves almost no degradation in its optical modulation contrast with the device showing 22.9% contrast and the spectra for these two folding states are almost overlapping. After 50 folding cycles, there is a slight reduction in optical contrast with the final contrast of 21.4%.

The effect of folding on the color switching rate is shown in Figure 4h, the switching curves for 0 cycle and 5 cycles are almost overlapping. The $T_{coloring}$ and $T_{bleaching}$ at 0 folding are 4.5 and 11.2 s, respectively. The $T_{coloring}$ and $T_{bleaching}$ after 5 folding cycles are 4.8 and 11.4 s, respectively. The change in the switching response between these two folding states is negligible. After 50 cycles of folding, the device gives a $T_{coloring}$ and $T_{bleaching}$ 6.8 and 13.2 s, respectively. The response time has only slightly increased, which manifested the excellent foldability of the electrochromic nanopaper.

Due to the more rigid and dense WO_3 film that wraps around the Ag nanowires after electrodeposition, some Ag nanowires were found to be delaminated from the nanopaper substrate following the compressive breakage of WO_3 after the 50 cyclic folding as evidenced in Figure S8f, Supporting Information. The presence of WO_3 protrusions will degrade the conductivity across the crease. This results in a comparatively slower kinetics in area B in Figure S8g (Supporting Information) showing a slower switching rate, and some loss of active electrochrome

at the crease after folding. For the sample folded for 5 cycles (Figure S8e, Supporting Information), except for a slight crack due to internal compressive stress build-up, there is negligible electrochromic performance degradation.

3. Conclusion

A highly efficient nanopaper transfer method has been demonstrated in this work to fabricate nanopaper electrodes. Transparent conductive foldable nanopaper electrodes with ultrahigh figure of merit have been obtained. Foldable electrochromic nanopaper has also been demonstrated. The transparent nanopaper is helpful in enhancing the coloration efficiency and cycling stability of the electrodeposited WO_3 electrochromism. The excellent performance of the electrochromic nanopaper is promising as the next generation reflective e-paper or display. This nanopaper electrode as well as the facile and efficient nanopaper transfer method holds great promise for applications to future generation deformable electronics.

4. Experimental Section

Nanopaper Electrode Fabrication: 0.5 g 3 wt% nanocellulose with diameter of 22 nm and length of 1 μm (University of Maine, USA) was dispersed in 100 mL DI water. Ag nanowires (Seashell Technology, USA) with diameters of 40–100 nm and lengths of 20–100 μm were diluted to 0.025 mg mL^{-1} in ethanol. Ag nanowires were first vacuum-filtrated onto a polycarbonate filter membrane (Millipore GTTP, pore size 220 nm) to form the first conductive layer. Nanocellulose suspension is gently poured over the first layer to conformally cover all the nanowires and forms the second nanopaper layer. The whole system is kept at 105 °C to evaporate the water and let the nanocellulose assemble into a dense strong nanopaper layer. Finally, the nanopaper layer was peeled off from the membrane with a highly conductive Ag nanowire network layer successfully transferred onto the nanopaper surface.

WO_3 Deposition: A typical electrochemical deposition of WO_3 onto the nanopaper electrode is carried out. The precursor for WO_3 deposition is prepared as follows. 1.8 g tungsten powder (Alfa Aeser, USA) is dissolved into H_2O_2 solution (30%, 60 mL, Tokyo Chemical Industry, Japan) and later stirred continuously for 12 h. The deposition is performed at –0.7 V under a three electrode configuration with Ag/AgCl as the reference and Pt plate as the counter. The voltage supply is from Solartron 1470E.

Characterization: The morphology of nanocellulose and fabricated nanopaper electrode is investigated on a field emission scanning electron microscopy (FESEM) JEOL 7600F. The sample roughness is measured using an atomic force microscope (AFM) with a DI 3100. Conductivity of the nanopaper electrode is evaluated by measuring the sheet resistance on a CMT-SR2000N four point probe. The diffusive transmittance is measured with an integrating sphere attachment in an UV–vis spectrophotometer (Shimadzu UV-3600).

Electrochromic Performance Testing: The electrochromic property of the WO_3 deposited nanopaper electrode was assessed under two electrode configuration (Pt wire as the reference and counter) in reflective mode with the reflective signal gathered inside the integrating sphere. The color switching was induced by polarizing the electrochromic nanopaper between –1.8 and –0.2 V versus the reference electrode in 1 M H_2SO_4 electrolyte.

Supporting Information

Supporting Information is available from the Wiley Online Library or from the author.

Acknowledgements

This work is supported by the Competitive Research Programme (NRF-CRP13-2014-02) under the National Research Foundation, Prime Minister's Office, Singapore. W. Kang acknowledges the scholarship awarded by Nanyang Technological University.

Received: February 7, 2015
Revised: April 27, 2015
Published online: May 26, 2015

[1] P. M. Monk, R. J. Mortimer, D. R. Rosseinsky, *Electrochromism: Fundamentals and Applications*, John Wiley & Sons, Weinheim, Germany **2008**.
[2] W. Kang, C. Yan, X. Wang, C. Y. Foo, A. W. M. Tan, K. J. Z. Chee, P. S. Lee, *J. Mater. Chem. C* **2014**, *2*, 4727.
[3] C. Yan, W. Kang, J. Wang, M. Cui, X. Wang, C. Y. Foo, K. J. Chee, P. S. Lee, *ACS Nano* **2013**, *8*, 316.
[4] Z. Wu, Z. Chen, X. Du, J. M. Logan, J. Sippel, M. Nikolou, K. Kamaras, J. R. Reynolds, D. B. Tanner, A. F. Hebard, *Science* **2004**, *305*, 1273.
[5] D. Zhang, K. Ryu, X. Liu, E. Polikarpov, J. Ly, M. E. Tompson, C. Zhou, *Nano Lett.* **2006**, *6*, 1880.
[6] X. Li, Y. Zhu, W. Cai, M. Borysiak, B. Han, D. Chen, R. D. Piner, L. Colombo, R. S. Ruoff, *Nano Lett.* **2009**, *9*, 4359.
[7] S. Bae, H. Kim, Y. Lee, X. Xu, J.-S. Park, Y. Zheng, J. Balakrishnan, T. Lei, H. R. Kim, Y. I. Song, *Nat. Nanotechnol.* **2010**, *5*, 574.
[8] G.-X. Ni, Y. Zheng, S. Bae, C. Y. Tan, O. Kahya, J. Wu, B. H. Hong, K. Yao, B. Ozyilmaz, *ACS Nano* **2012**, *6*, 3935.
[9] L. Hu, H. S. Kim, J.-Y. Lee, P. Peumans, Y. Cui, *ACS Nano* **2010**, *4*, 2955.
[10] H. Wu, D. Kong, Z. Ruan, P.-C. Hsu, S. Wang, Z. Yu, T. J. Carney, L. Hu, S. Fan, Y. Cui, *Nat. Nanotechnol.* **2013**, *8*, 421.
[11] A. R. Rathmell, M. Nguyen, M. Chi, B. J. Wiley, *Nano Lett.* **2012**, *12*, 3193.
[12] H. Wu, L. Hu, M. W. Rowell, D. Kong, J. J. Cha, J. R. McDonough, J. Zhu, Y. Yang, M. D. McGehee, Y. Cui, *Nano Lett.* **2010**, *10*, 4242.
[13] M. Layani, P. Darmawan, W. L. Foo, L. Liu, A. Kamyshny, D. Mandler, S. Magdassi, P. S. Lee, *Nanoscale* **2014**, *6*, 4572.
[14] S. H. Ahn, L. J. Guo, *Nano Lett.* **2010**, *10*, 4228.
[15] K. Zilberberg, F. Gasse, R. Pagui, A. Polywka, A. Behrendt, S. Trost, R. Heiderhoff, P. Görrn, T. Riedl, *Adv. Funct. Mater.* **2014**, *24*, 1671.
[16] M.-S. Lee, K. Lee, S.-Y. Kim, H. Lee, J. Park, K.-H. Choi, H.-K. Kim, D.-G. Kim, D.-Y. Lee, S. Nam, J.-U. Park, *Nano Lett.* **2013**, *13*, 2814.
[17] C. Preston, Z. Fang, J. Murray, H. Zhu, J. Dai, J. N. Munday, L. Hu, *J. Mater. Chem. C* **2014**, *2*, 1248.
[18] J. van de Groep, P. Spinelli, A. Polman, *Nano Lett.* **2012**, *12*, 3138.
[19] C. Yang, H. Gu, W. Lin, M. M. Yuen, C. P. Wong, M. Xiong, B. Gao, *Adv. Mater.* **2011**, *23*, 3052.
[20] C. Yan, J. Wang, X. Wang, W. Kang, M. Cui, C. Y. Foo, P. S. Lee, *Adv. Mater.* **2014**, *26*, 2022.
[21] F. Jiang, Y.-L. Hsieh, *Carbohydrate Polym.* **2013**, *95*, 32.
[22] H. Koga, T. Saito, T. Kitaoka, M. Nogi, K. Suganuma, A. Isogai, *Biomacromolecules* **2013**, *14*, 1160.
[23] M. Henriksson, G. Henriksson, L. Berglund, T. Lindström, *Eur. Poly. J.* **2007**, *43*, 3434.
[24] H. Koga, M. Nogi, N. Komoda, T. T. Nge, T. Sugahara, K. Suganuma, *NPG Asia Mater.* **2014**, *6*, e93.
[25] J. Huang, H. Zhu, Y. Chen, C. Preston, K. Rohrbach, J. Cumings, L. Hu, *ACS Nano* **2013**, *7*, 2106.
[26] L. Hu, G. Zheng, J. Yao, N. Liu, B. Weil, M. Eskilsson, E. Karabulut, Z. Ruan, S. Fan, J. T. Bloking, *Energy Environ. Sci.* **2013**, *6*, 513.

[27] Y. Fujisaki, H. Koga, Y. Nakajima, M. Nakata, H. Tsuji, T. Yamamoto, T. Kurita, M. Nogi, N. Shimidzu, *Adv. Funct. Mater.* **2014**, *24*, 1657.
[28] M. Nogi, N. Komoda, K. Otsuka, K. Suganuma, *Nanoscale* **2013**, *5*, 4395.
[29] H. Zhu, Z. Jia, Y. Chen, N. Weadock, J. Wan, O. Vaaland, X. Han, T. Li, L. Hu, *Nano Lett.* **2013**, *13*, 3093.
[30] Z. Gui, H. Zhu, E. Gillette, X. Han, G. W. Rubloff, L. Hu, S. B. Lee, *ACS Nano* **2013**, *7*, 6037
[31] B. M. Novak, *Adv. Mater.* **1993**, *5*, 422.
[32] H. Yano, J. Sugiyama, A. N. Nakagaito, M. Nogi, T. Matsuura, M. Hikita, K. Handa, *Adv. Mater.* **2005**, *17*, 153.
[33] Z. Fang, H. Zhu, C. Preston, X. Han, Y. Li, S. Lee, X. Chai, G. Chen, L. Hu, *J. Mater. Chem. C* **2013**, *1*, 6191.
[34] Z. Fang, H. Zhu, Y. Yuan, D. Ha, S. Zhu, C. Preston, Q. Chen, Y. Li, X. Han, S. Lee, *Nano Lett.* **2014**, *14*, 765.
[35] H. Zhu, Z. Xiao, D. Liu, Y. Li, N. J. Weadock, Z. Fang, J. Huang, L. Hu, *Energy Environ. Sci.* **2013**, *6*, 2105.
[36] H. Zhu, S. Parvinian, C. Preston, O. Vaaland, Z. Ruan, L. Hu, *Nanoscale* **2013**, *5*, 3787.
[37] K. S. Kim, Y. Zhao, H. Jang, S. Y. Lee, J. M. Kim, K. S. Kim, J.-H. Ahn, P. Kim, J.-Y. Choi, B. H. Hong, *Nature* **2009**, *457*, 706.
[38] J. Song, F.-Y. Kam, R.-Q. Png, W.-L. Seah, J.-M. Zhuo, G.-K. Lim, P. K. Ho, L.-L. Chua, *Nat. Nanotechnol.* **2013**, *8*, 356.
[39] J. W. Suk, A. Kitt, C. W. Magnuson, Y. Hao, S. Ahmed, J. An, A. K. Swan, B. B. Goldberg, R. S. Ruoff, *ACS Nano* **2011**, *5*, 6916.
[40] K. Parvez, R. Li, S. R. Puniredd, Y. Hernandez, F. Hinkel, S. Wang, X. Feng, K. Müllen, *ACS Nano* **2013**, *7*, 3598.
[41] A. Kaskela, A. G. Nasibulin, M. Y. Timmermans, B. Aitchison, A. Papadimitratos, Y. Tian, Z. Zhu, H. Jiang, D. P. Brown, A. Zakhidov, *Nano Lett.* **2010**, *10*, 4349.
[42] A. R. Madaria, A. Kumar, F. N. Ishikawa, C. Zhou, *Nano Res.* **2010**, *3*, 564.
[43] S. J. Kang, B. Kim, K. S. Kim, Y. Zhao, Z. Chen, G. H. Lee, J. Hone, P. Kim, C. Nuckolls, *Adv. Mater.* **2011**, *23*, 3531.
[44] D. Hines, S. Mezhenny, M. Breban, E. Williams, V. Ballarotto, G. Esen, A. Southard, M. Fuhrer, *Appl. Phys. Lett.* **2005**, *86*, 163101.
[45] R. A. Ryntz, P. V. Yaneff, *Coatings of Polymers and Plastics*, CRC Press, New York, USA **2003**.
[46] S. Wu, *Polymer Interface and Adhesion*, CRC Press, New York, USA **1982**.
[47] Y. Peng, D. J. Gardner, Y. Han, Z. Cai, M. A. Tshabalala, *J. Colloid Inter. Sci.* **2013**, *405*, 85.
[48] K. Missoum, M. N. Belgacem, J. Bras, *Materials* **2013**, *6*, 1745.
[49] I. A. Sacui, R. C. Nieuwendaal, D. J. Burnett, S. J. Stranick, M. Jorfi, C. Weder, E. J. Foster, R. T. Olsson, J. W. Gilman, *ACS Appl. Mater. Inter.* **2014**, *6*, 6127.
[50] F. L. Leite, C. C. Bueno, A. L. Da Róz, E. C. Ziemath, O. N. Oliveira, *Int. J. Mol. Sci.* **2012**, *13*, 12773.
[51] M. N'Gom, J. Ringnalda, J. F. Mansfield, A. Agarwal, N. Kotov, N. J. Zaluzec, T. B. Norris, *Nano Lett.* **2008**, *8*, 3200.
[52] Q. N. Luu, J. M. Doorn, M. T. Berry, C. Jiang, C. Lin, P. S. May, *J. Colloid Inter. Sci.* **2011**, *356*, 151.
[53] D. S. Hecht, L. Hu, G. Irvin, *Adv. Mater.* **2011**, *23*, 1482.
[54] S. De, T. M. Higgins, P. E. Lyons, E. M. Doherty, P. N. Nirmalraj, W. J. Blau, J. J. Boland, J. N. Coleman, *ACS Nano* **2009**, *3*, 1767.
[55] M. Dressel, *Electrodynamics of Solids: Optical Properties of Electrons in Matter*, Cambridge University Press, Cambridge, England **2002**.
[56] S. De, P. J. King, P. E. Lyons, U. Khan, J. N. Coleman, *ACS Nano* **2010**, *4*, 7064.
[57] Y. Lu, L. Liu, W. Foo, S. Magdassi, D. Mandler, P. S. Lee, *J. Mater. Chem. C* **2013**, *1*, 3651.
[58] R. P. Tandon, S. Hotchandani, *Phys. Status Solidi* **2001**, *185*, 453.
[59] Z. Hu, Z. Ji, W. W. Lim, B. Mukherjee, C. Zhou, E. S. Tok, C.-H. Sow, *ACS Appl. Mater. Inter.* **2013**, *5*, 4731.